

# Feedforward Inversion Control of DC/DC Dual-Bridge Series Resonant Converter in Buck and Boost Modes

Alex Borisevich, akpc806b@gmail.com,  
 Filipp Gleyzer, gleyzerf@smccd.edu,  
 Valeria Gavrilenko, gavv00@vse.cz

December 21, 2024

## Abstract

In the paper, a nonlinear inversion technique for the steady-state model of the active dual-bridge series resonant converter is presented. The obtained control strategy allows cycle averaged output current regulation and performs waveform alignment for the controllable achievement of ZVS and synchronous rectification. The control is valid both for voltage buck and boost operating modes, as well as for low-power operation at a fixed frequency. Robustness of the control is studied by simulations with external linear control loops.

## 1 Introduction

The dual-bridge series resonant converter (DB SRC) [1], which shares some similarities with the standard full-bridge DC/DC series resonant converters (like LLC), still has some unique features due to the secondary-side bridge, such as the capability of bidirectional power flow and voltage boost operation. Such type of converter topology is particularly promising for electric vehicles chargers applications [1-3], including off-board charging stations and on-board charger modules with an ability for bidirectional vehicle-to-grid power flow. Additionally, many other power electronics applications like battery energy storage and DC line power transmission are target areas of DB SRC topology.

The modulation scheme for DB SRC usually enables pure ZVS on the primary side, and combined ZVS/ZCS on the secondary side, and allows for an efficient utilization of the primary side switches with wide changes in load or supply voltage, which is preferred in many applications [2]. The impedance of series resonant tank is determined by value of inductor and capacitor together with the switching frequency. Therefore, it can operate at higher frequency under high power level [3] than just dual active bridge topologies without resonant capacitor, which allows more compact magnetic designs.

All the switches in the two bridges work with 50

Comparing to LLC converter, the DB SRC converter requires more advanced control strategy since the DC gain of a LC series resonant converter is always less than unity with a passive (diode) rectifier. Also at light-load condition, the impedance of the load is very large compared to the impedance of the resonant network, so all the input voltage is imposed on the load [5]. Thus an actively controlled full bridge on the secondary side is essential in order to achieve voltage gain higher than one and regulate power delivered at light load.

The operating modes and controls principles of the converter have been extensively analyzed in [6, 7, 8]. The published modeling efforts can be classified into three categories:

1. Fundamental harmonics approximation (FHA) approach [6, 7, 8, 9, 10], consisting of replacement the rectangular voltage waveforms by sinusoidal approximations, calculated accordingly. The same result can be achieved if output and input voltages are represented by rotating vectors using phasor diagrams. If the analysis of a converter is performed not too far from its resonant frequency, then the resonant tank current consists primary a fundamental harmonic, and this method produces reasonable well approximations. Another advantage of FHA is that this method ends up with trigonometric functions over switching parameters, where analytical results can be relevantly easy to obtain.

2. State-plane trajectory analysis pioneered by R. Oruganti [12] and used by many followers [13, 14, 15, 16].. The key idea is to represent the converter dynamics in two-dimensional plane of resonant inductor current and resonant capacitor voltage. The analysis is greatly simplified by the fact that with a proper normalization the state plane trajectory of voltage step response of an undamped LC circuit is circular and is centered at the DC solution of the circuit. Thus, accurate and purely geometric analysis can be performed for arbitrary operating point and switching pattern. The downside of this method is that the closed form solutions are becoming very complicated with less trivial PWM patterns (like combined duty cycle and phase shift control), and also for multi-element resonant converters, more state variables need to be analyzed and more complicated calculation is required.

3. Piece-wise time-domain modeling. This technique is originally applied to the dual-bridge converters [17, 18, 19, 20] without a resonant tank, where transformer current is a straight line between switching events. Thus each time interval between switching of bridges can be analyzed separately, and then final waveform is obtained by gluing together transient responses for consequential time intervals. This technique can be directly obtained to series resonant converter operating very far from resonant frequency, where resonant tank current is piece-wise linear. Also it is not very hard to obtain a closed form solutions for different operating modes of series resonant converter [21].

Despite pretty diverse modeling and control techniques published, there are still some gaps, namely:

- there is no model and corresponding nonlinear control problem formulated addressing both produced output power and optimal regime of operation in terms of the waveform timings,
- all three modes of operation, namely variable frequency buck, variable frequency boost and fixed frequency low power operation are not being considered in a single model.

In this work we will derive nonlinear control affine model of the converter, which describes large signal operation over whole frequency range above resonance and in all possible operation modes as buck, boost and low power. This model also demonstrates interesting control properties of the converter like high nonlinearity respect to the switching parameters, singularity of output current surface between buck and boost modes, and also holonomic constraints for control variables. We believe that this model could be an another practical benchmark for many advanced nonlinear control techniques such as feedback linearization, differential flatness theory, optimal control, etc.

## 2 Background

This section is a recall of previously published results, and the model [22] in particularly.

### 2.1 The converter topology

The basic electrical circuit of the series LC resonant DC/DC converter is shown in Figure 1.

The circuit consists of two full (H) transistor bridges: input bridge with switches  $S_1$ – $S_4$  and output bridge with switches  $S_5$ – $S_8$ . The output bridge is directly connected to the secondary side of transformer TX. The input bridge is connected to the transformer TX through capacitor C. Simple representation of transformer is used with magnetizing inductance  $L_m$ , leakage inductance  $L$  and an ideal transformer with turns ratio  $n$ .

If the magnetizing inductance  $L_m$  is much larger than leakage inductance  $L$ :  $L_m \gg L$ , then there is almost no circulating magnetizing current in the circuit. This has an advantage because all the current from primary side is flowing to the secondary side which increases the efficiency. Also the current in secondary side of transformer is in phase with primary side, which allows easy synchronous rectification by measuring current only in primary side.

By eliminating  $L_m$  from the circuit, we can spot that the stray inductance  $L$  together with capacitor  $C$  forms LC resonant tank. Also ideal transformer can be embedded into secondary bridge for simplification of analysis. Thus we can obtain a black-box circuit presented in Figure 1.

The alternating current which flows through the leakage inductance and resonant capacitor is called tank current  $i_t(t)$ . This current is being rectified by secondary transistor bridge and assuming that all the ripple components are blocked by output filter capacitors (not shown in Figure 1), a direct current  $I_{out}$  is induced through a load.

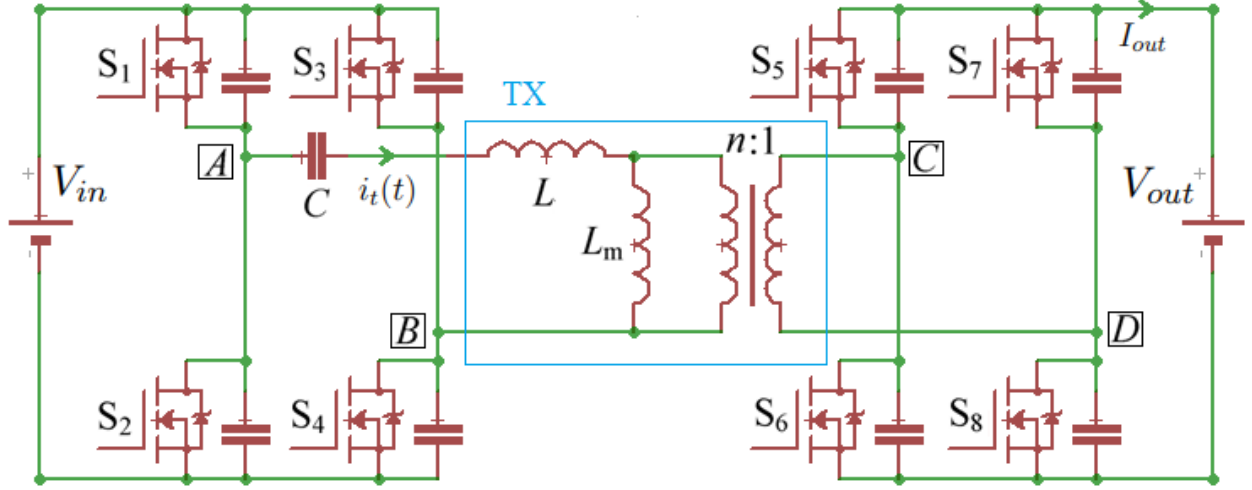


Figure 1: DC/DC circuit.

## 2.2 The voltage waveforms

Let's consider voltages  $v_{in}(t)$  and  $v_{out}(t)$  at output terminals of bridges in the circuit 1.

- The voltage  $v_{in}(t)$  corresponds to a voltage measured between points A–B of input bridge.
- The voltage  $v_{out}(t)$  corresponds to scaled by  $n$  voltage measured between points C–D of output bridge.

Effectively, these voltage  $v_{in} - v_{out}$  is applied to LC-circuit. Figure 2 shows the real and rectangular approximated voltages.

Let's consider rectangular approximated voltages  $u_{in}(t)$  and  $u_{out}(t)$  for easier explanation of controllable switching parameters:

- The input voltage source is producing rectangular pulses with controlled duty cycle and frequency. The amplitude of pulse is  $V_{in}$  and the on-time is  $d$  (in radians, i.e.  $d = \pi$  is full square wave). The angular frequency is  $\omega$ , which is equivalent to frequency  $F = 1/T$  in Hz.
- The output voltage source is producing rectangular pulses with amplitude  $nV_{out}$  with controlled duty cycle, frequency, and phase shift respect to input bridge. The reciprocal of duty cycle, the off-time or short time is  $s$  (defined in radians,  $s = \pi$  means that secondary side of transformer is fully shorted). The off-time is always located at the beginning of switching cycle. The phase shift between the output bridge switching cycle and input bridge switching cycle is  $\beta$ .

The output to input voltage ratio is defined as converter voltage gain:

$$G = \frac{nV_{out}}{V_{in}} \quad (1)$$

The real waveforms are looking differently than approximated ones because of dead times, which are smoothing rising and falling edges of the switching pulses. Since this DC/DC belongs to the class of resonant converters, energy is also transferring during the dead time, and the dead time is an essential phase of converter operation.

The duration of dead-time for input bridge is  $T_D^{in}$ , and the duration of dead-time for output bridge is  $T_D^{out}$ .

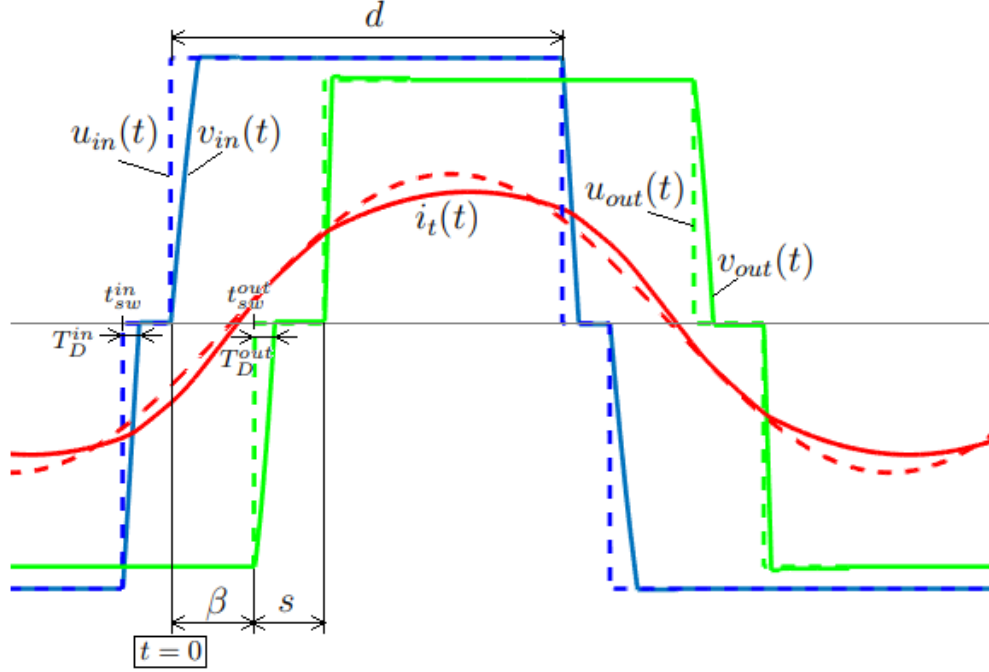


Figure 2: Real and approximated voltages applied to resonant LC circuit and PWM parameters.

### 2.3 The model

The converter model obtained in [22] by first harmonic approximation of tank current can be summarized as:

$$W = \frac{I_{out}}{V_{in}} = \frac{n}{2\pi^2} \frac{\sqrt{A^2 + B^2}}{Z(\omega)} (\cos(s + \delta) + \cos \delta) \quad (2)$$

where coefficients  $A$  and  $B$  along with timing quantities  $\sigma$  and  $\delta$  are given as

$$\begin{aligned} A &= 4 \sin d + 4G \sin(\beta + s) + 4G \sin \beta \\ B &= 4 - 4G \cos(\beta + s) - 4G \cos \beta - 4 \cos d \\ \sigma &= \text{atan2}(B, A), \quad \delta = \beta - \sigma \end{aligned} \quad (3)$$

and  $Z(\omega)$  is resonant LC tank impedance:

$$Z(\omega) = X_L - X_C = \omega L - \frac{1}{\omega C} \quad (4)$$

The timing quantities  $\sigma$ ,  $\delta$  and  $\beta$  are shown in Figure 3  
Namely:

- The  $\sigma$  is an angular time (in radians) from the rising edge of positive input bridge voltage  $v_{in}(t)$  to a moment when the tank current crosses 0 level:  $i_t = 0$ . I.e. formally,  $i_t(\sigma/\omega) = 0$ .
- The  $\delta$  is an angular time (in radians) from the moment when the tank current crosses 0 level  $i_t = 0$  to the rising edge of positive output bridge voltage  $v_{out}(t)$ .

It is pretty obvious that:

$$\sigma + \delta = \beta \quad (5)$$

Worth noting that both  $\sigma$  and  $\delta$  are signed.

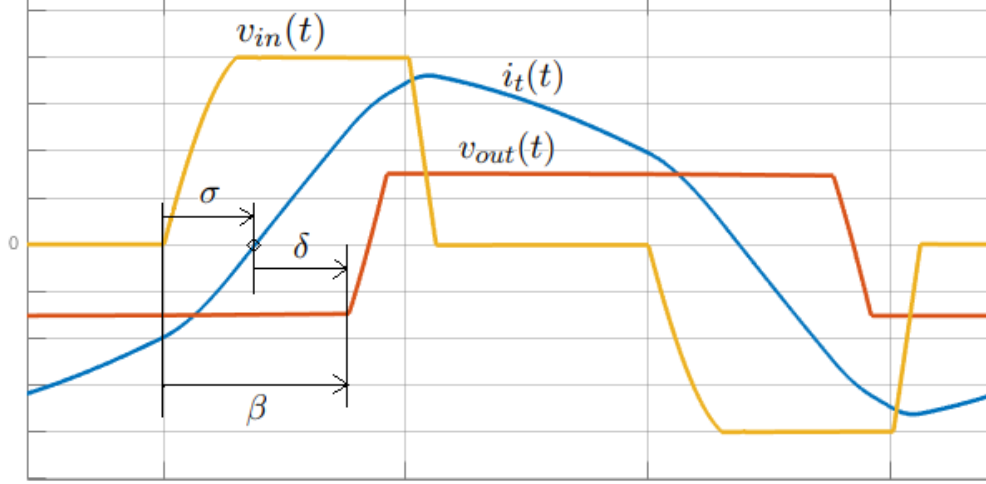


Figure 3: Timing of input and output voltages respect to tank current zero level crossing.

## 2.4 Regulation problem and optimality metrics

In this particular work the DC/DC converter will be represented as a current source. This particular representation covers EV battery charger applications, which is main application area of such topologies.

Thus, an output DC current problem regulation can be formulated as follows:

*Find PWM switching parameters:  $d, s, \beta, \omega$  in order to achieve desired steady-state output current:*

$$I_{out}(d, s, \beta, \omega) = I_{out}^* \quad (6)$$

where  $I_{out}^*$  is reference desired value of output current.

Sine the converter topology considered here is lossless, some additional facts need to be considered for derivation of optimality conditions. The following requirements can be fulfilled in order to operate the converter efficiently:

- Conduction loss minimization.

In order to minimize conduction loss, the amplitude (or RMS) value  $I_t$  of tank current  $i_t(t)$  needs to be minimized. Thus every set of switching parameters ( $d, s, \beta, \omega$ ) can be evaluated for conduction loss optimality:

$$\frac{I_t}{I_{out}} \rightarrow \min \quad (7)$$

- Turn-on switching loss minimization.

The topology under consideration can be operating in soft-switching mode, which minimizes turn-on losses down to zero. The conditions for soft-switching discussed in many studies. Necessary conditions can be summarized in two statements:

1. A rising edge of positive  $v_{in}(t)$  should be at negative tank current  $i_t(t)$ .
2. A rising edge of positive  $v_{out}(t)$  should be at positive tank current  $i_t(t)$ .

These two statements can be summarized with respect to the timing of switching events. Let's assume that  $t = 0$  during positive rising edge of  $v_{in}(t)$ . Then the soft switching conditions for turn-off are:

$$i_t(0) \leq 0, \quad i_t(\beta/\omega) \geq 0 \quad (8)$$

or using angular quantities defined in Figure 3:

$$\sigma \geq 0, \delta \geq 0 \quad (9)$$

- Turn-off switching loss minimization.

For the turn-off losses, a true soft-switching can't be achieved in this topology. The turn-off losses can be only mitigated. One practical approach is to use a capacitive snubber across the MOSFETs. Additionally, turning-off close to zero current, i.e. achieving ZCS commutation is usually helps achieve better efficiency.

Thus, we can introduce the following criteria:

$$|i_t(0)| \rightarrow \min, |i_t(\beta/\omega)| \rightarrow \min \quad (10)$$

It worth noting, that commutating at zero current, i.e. achieving an obvious goal  $i_t(0) = i_t(\beta/\omega) = 0$  is not practical since ZVS can be achieved only at specific current levels which allow discharge of internal Coss and external snubber capacitors (if any) during a dead-time interval.

So generally speaking, the following constraints need to be satisfied:

$$i_t(0) = -I_{th}^{in}, i_t(\beta/\omega) = I_{th}^{out} \quad (11)$$

where  $I_{th}^{in}, I_{th}^{out} \geq 0$  are threshold currents for commutation of input and output bridges correspondingly.

## 2.5 The output control problem reformulation

Let's follow the discussion from section 2.4 by taking into account model equations (2).

First, achieving the desired output current  $I_{out}^*$  is the same as regulating to a prescribed transconductance  $W^* = I_{out}^*/V_{in}$  for a given input voltage  $V_{in}$ . So the reformulated output control problem is to find switching parameters  $d, s, \beta, \omega$  so that:

$$W(d, s, \beta, \omega) = W^* \quad (12)$$

where function  $W(d, s, \beta, \omega)$  is given by (2).

Additionally, from [22] it is known that the amplitude of tank current is given as:

$$I_t = \frac{V_{in}}{2\pi Z} \sqrt{A^2 + B^2} \quad (13)$$

Using this, the ratio of  $I_t/I_{out}$  can be expressed as:

$$\frac{I_t}{I_{out}} = \frac{\pi}{n} \cdot \frac{1}{\cos(s + \delta) + \cos \delta} \quad (14)$$

The ratio  $I_t/I_{out}$  is minimized when denominator term  $\cos(s + \delta) + \cos \delta$  is maximized. Its maximal value 2 is achieved when both  $\delta = 0$  and  $s = 0$ .

So the optimality for tank current amplitude can be formulated as follows:

$$\frac{I_t}{I_{out}} \rightarrow \min \iff \begin{cases} \delta \rightarrow \min \\ s \rightarrow \min \end{cases} \quad (15)$$

This result can be physically interpreted as minimization of reactive power in the resonant tank. Furthermore, the case of  $\delta = 0$  corresponds to ideal synchronous rectification by the secondary output bridge, i.e. when voltage waveform is fully aligned with tank current.

This type of control which uses phase shift control of the secondary side PWM pulses to align the commutation of the secondary bridge with the sign of the resonant tank is known as *indirect* or PLL-based synchronous rectification [23]. In contrast with conventional *direct* synchronous rectification in which the switching of the secondary side is driven by a sign of the resonant tank current detected by a comparator.

The advantages of indirect synchronous rectification to the direct one are twofold:

1. It is possible to compensate comparator's and gate driver's delay by switching the secondary side before the resonant tank current flips polarity, which leads to efficiency increase by minimization of reactive power
2. Since the output of the current sign comparator is no longer driving the secondary side directly, the system is more prone to current measurement noise and potentially can function even without the current sensor (in open loop alignment control, assuming some margins on inefficiency).

### 3 Model inversion for commutation parameters $d, s, \beta$

#### 3.1 Nonlinear inversion problem formulation

In order to regulate waveform quantities  $\sigma$  and  $\delta$  to desired values that maximize efficiency, a control system needs to be implemented around the plant which takes  $d, s, \beta$  and outputs  $\sigma, \delta$  as measurable quantities.

A feedforward inversion approach is proposed below to linearize  $\sigma$  and  $\delta$  as functions of controllables  $d, s, \beta$ . Thus, the following nonlinear inversion problem can be formulated in form of a system of nonlinear equations:

$$\begin{aligned}\sigma(d, s, \beta, G) &= \sigma^* \\ \delta(d, s, \beta, G) &= \delta^*\end{aligned}\tag{16}$$

with respect to unknown variables  $d \in [0, \pi]$ ,  $s \in [0, \pi]$ ,  $\beta \in [-\pi, \pi]$  and for given referenced values  $\sigma^* \in [-\pi/2, \pi/2]$ ,  $\delta^* \in [-\pi/2, \pi/2]$  and parameter  $G \geq 0$ .

The concept of nonlinear inversion can be illustrated by a block diagram in Figure 4, where nonlinear function  $F$  is given by model equations (3) and  $F^{-1}$  is a solution of (16).

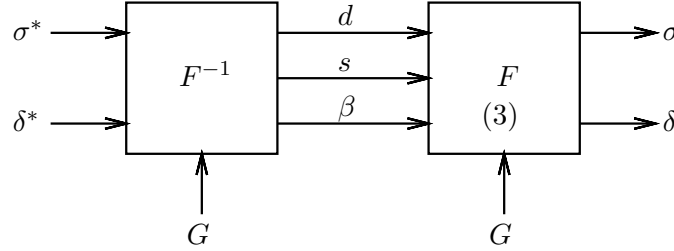


Figure 4: Nonlinear inversion with respect to  $\sigma$  and  $\delta$ .

In order to overcome uncertainties of the model (3), an additional external (linear) feedback controller should be used in conjunction to decoupling and linearization as a solution of (16). These two controllers could have PID form and regulate  $\sigma$  and  $\delta$  independently as shown in Figure 5.

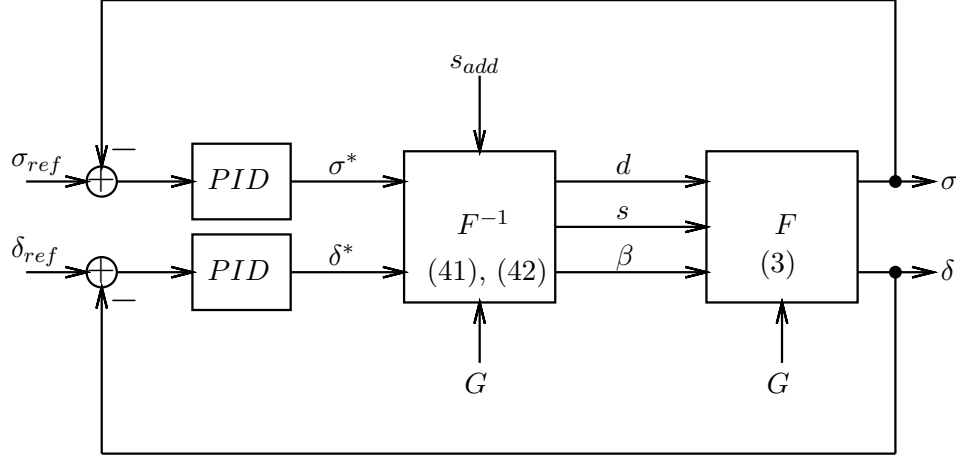


Figure 5: Architecture of control system for  $\sigma$  and  $\delta$ .

### 3.2 Nonlinear inversion condition

Let's recall (3) as  $\sigma^* = \text{atan2}(B, A)$ . In order to have  $\sigma^* \in [-\pi/2, \pi/2]$ , the argument  $A$  should not be negative:

$$A = \sin d + G \sin(\beta + s) + G \sin \beta \geq 0 \quad (17)$$

If this holds, then  $\text{atan2}$  can be replaced by  $\tan$ , and the nonlinear inversion problem can be rewritten as following two equations:

$$\frac{1 - G \cos(\beta + s) - G \cos \beta - \cos d}{\sin d + G \sin(\beta + s) + G \sin \beta} = \tan \sigma^* \quad (18)$$

$$\delta^* + \sigma^* = \beta$$

Note that  $\beta = \delta^* + \sigma^*$  became constant.

This can be transformed as follows:

$$\tan \sigma^* \cdot (G \sin(\beta + s) + G \sin \beta + \sin d) + G \cos(\beta + s) + G \cos \beta + \cos d - 1 = 0 \quad (19)$$

And the equation can be simplified further by using identity of harmonic addition:

$$\tan \sigma^* \sin(x) + \cos(x) = \sqrt{(\tan \sigma^*)^2 + 1} \cdot \cos(x - \text{atan} \tan \sigma^*) = \sqrt{(\tan \sigma^*)^2 + 1} \cdot \cos(x - \sigma^*) \quad (20)$$

where  $x$  is an arbitrary angular argument.

Taking into account the following trigonometric identity:

$$\frac{1}{\sqrt{(\tan \sigma^*)^2 + 1}} = |\cos \sigma^*| \quad (21)$$

and using harmonic addition, the nonlinear inversion condition can be rewritten as:

$$G \cos(\beta + s - \sigma^*) + G \cos(\beta - \sigma^*) + \cos(d - \sigma^*) - \cos \sigma^* = 0 \quad (22)$$

Note that the absolute value of  $\cos \sigma^*$  is safely omitted since the range of  $\sigma^*$  is  $[-\pi/2, \pi/2]$ .

Finally, using  $\beta = \delta^* + \sigma^*$ , it simplifies even further, which we will refer as *nonlinear inversion condition* (for  $d$  and  $s$ ):

$$G \cos(\delta^* + s) + G \cos \delta^* + \cos(d - \sigma^*) - \cos \sigma^* = 0 \quad (23)$$

It is important to note that (23) is underdetermined since it has two unknown variables  $d$  and  $s$ . So in order to find a unique solution, the minimization of  $s \rightarrow \min$  should be additionally imposed.



### 3.2.1 Buck mode with $s = 0$

This is the simplest mode of operation and obviously satisfies minimization condition since the  $s = 0$  is minimal value of  $s$ . Substituting this to (23)

$$2G \cos \delta^* + \cos(d - \sigma^*) - \cos \sigma^* = 0 \quad (24)$$

thus:

$$d = \arccos(\cos \sigma^* - 2G \cos \delta^*) + \sigma^* \quad (25)$$

The domain of this buck operating mode is given by domain of  $\arccos$  function and the range of  $d \in [0, \pi]$

$$\begin{aligned} -1 &\leq \cos \sigma^* - 2G \cos \delta^* \leq 1 \\ 0 &\leq \arccos(\cos \sigma^* - 2G \cos \delta^*) + \sigma^* \leq \pi \end{aligned} \quad (26)$$

Practically, since the  $\sigma^*$  is additive to result of  $\arccos$  in (25), it is pretty much possible that the calculation of  $d$  could give greater than  $\pi$  value. The boundary condition is

$$\cos \sigma^* - 2G \cos \delta^* = \cos(\pi - \sigma^*) = -\cos \sigma^* \quad (27)$$

and the domain for  $d \leq \pi$  is defined by inequality:

$$\cos \sigma^* \geq G \cos \delta^* \quad (28)$$

Another useful boundary case is when the argument of  $\arccos$  in (25) is out of  $[-1, 1]$  range, particularly for high values of  $G$ , which corresponds to a boost mode:

$$\cos \sigma^* - 2G \cos \delta^* = -1 \quad (29)$$

which translates to the following inequality:

$$\cos \sigma^* \geq 2G \cos \delta^* - 1 \quad (30)$$

### 3.2.2 Boost mode with $d = \pi$

Substituting  $d = \pi$  to (23) gives:

$$G \cos(\delta^* + s) + G \cos \delta^* - 2 \cos \sigma^* = 0 \quad (31)$$

thus for variable  $s$  it gives:

$$s = \arccos(2 \cos \sigma^* / G - \cos \delta^*) - \delta^* \quad (32)$$

The domain of this boost operating mode is given by domain of  $\arccos$  function and the range of  $s \in [0, \pi]$

$$\begin{aligned} -1 &\leq 2 \cos \sigma^* / G - \cos \delta^* \leq 1 \\ 0 &\leq \arccos(2 \cos \sigma^* / G - \cos \delta^*) - \delta^* \leq \pi \end{aligned} \quad (33)$$

Practically, since the  $\delta^*$  is additive to result of  $\arccos$  in (32), it is pretty much possible that the calculation of  $s$  could give negative value. The boundary condition is

$$2 \cos \sigma^* / G = 2 \cos \delta^* \quad (34)$$

and the domain for  $s \geq 0$  is defined by inequality:

$$\cos \sigma^* \leq G \cos \delta^* \quad (35)$$

Another useful boundary case is when the argument of  $\arccos$  in (25) is out of  $[-1, 1]$  range, particularly for low values of  $G$ , which corresponds to a buck mode:

$$2 \cos \sigma^* / G - \cos \delta^* = 1 \quad (36)$$

which translates to the following inequality:

$$2 \cos \sigma^* / G \leq 1 + \cos \delta^* \quad (37)$$

### 3.2.3 Explicit additive reference of $s$

There are use cases when both  $d < \pi$  and  $s > 0$  are required. In this case, value of  $s$  consists of two parts: a value required by (32) which will be denoted as  $s_{min}$  and an additive component  $s_{add} \geq 0$  which is specified externally:

$$s = s_{min} + s_{add} \quad (38)$$

It worth noting that just increasing  $s$  by addition of  $s_{min}$  without corresponding adjustment of  $d$  and  $\beta$  will change resulting  $\sigma$  and  $\delta$ . So in order to maintain prescribed  $\sigma^*$  and  $\delta^*$ , the  $d$  and  $\beta$  need to be adjusted.

Thus, the nonlinear inversion equation (23) needs to be modified as follows:

$$G \cos(\delta^* + s_{min} + s_{add}) + G \cos \delta^* + \cos(d - \sigma^*) - \cos \sigma^* = 0 \quad (39)$$

where  $s_{add}$  is a constant.

First consider the case of  $s_{min} = 0$ , which corresponds to the buck mode.

$$d = \arccos(\cos \sigma^* - G \cos(\delta^* + s_{add}) - G \cos \delta^*) + \sigma^* \quad (40)$$

The buck mode is defined by a condition of  $s_{min} = 0$  for any  $s_{add}$  including  $s_{add} = 0$ , which is the exactly the same condition as (28):  $\cos \sigma^* \geq G \cos \delta^*$ .

If buck mode with  $d \leq \pi$  and  $s = s_{add}$  is not feasible, then the boost mode is used. Minimal value of  $s$  without  $s_{add}$  is given by (32) which is

$$s_{min} = \arccos(2 \cos \sigma^* / G - \cos \delta^*) - \delta^* \quad (41)$$

Then in presence of  $s_{add} > 0$ , the value of  $d$  which satisfies inversion equation (39) needs to be calculated as follows:

$$d = \arccos(\cos \sigma^* - G \cos(\delta^* + s_{min} + s_{add}) - G \cos \delta^*) + \sigma^* \quad (42)$$

The last step in calculation of values  $d, s, \beta$  is to check inequality (17). If it is not satisfied, then the provided  $\delta^*$  and  $\sigma^*$  are not feasible.

### 3.3 Examples of feed-forward characteristics

#### 3.3.1 Buck mode $G = 0.5$

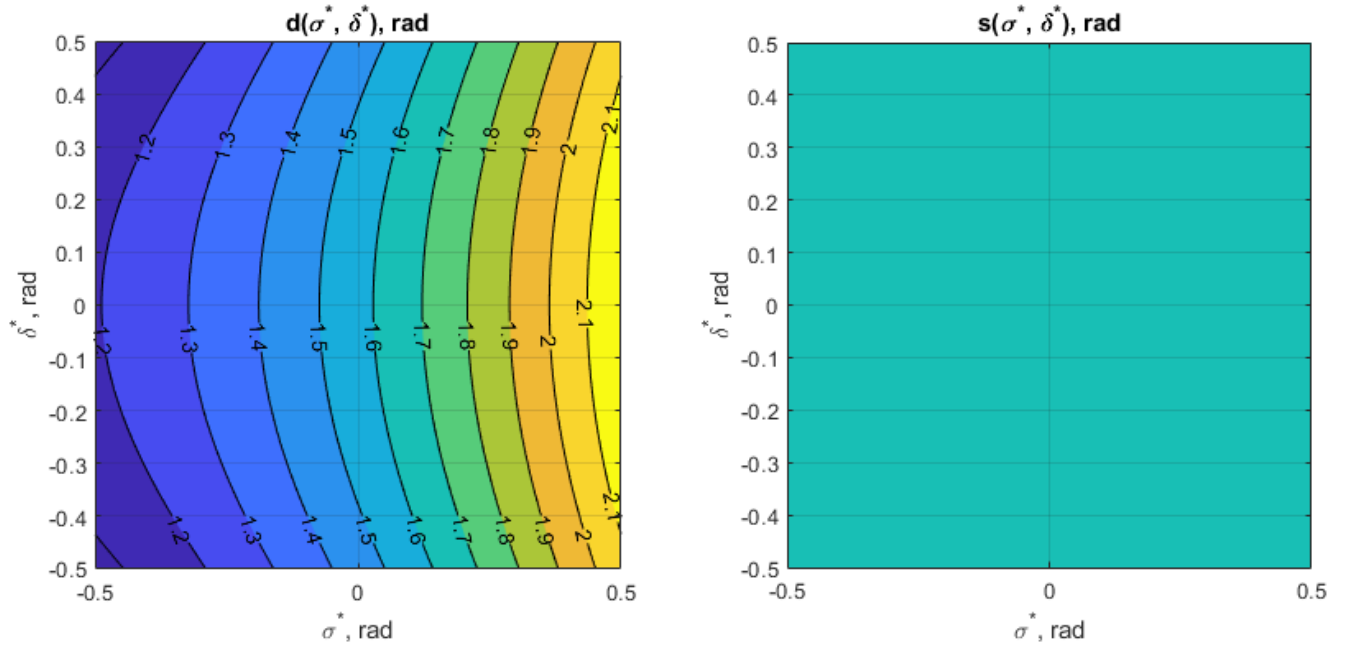


Figure 6: The switching waveform parameters  $d$  and  $s$  as functions of required  $\sigma$  and  $\delta$  for buck mode  $G = 0.5$  and  $s_{add} = 0$  (resulting in  $s = 0$ )

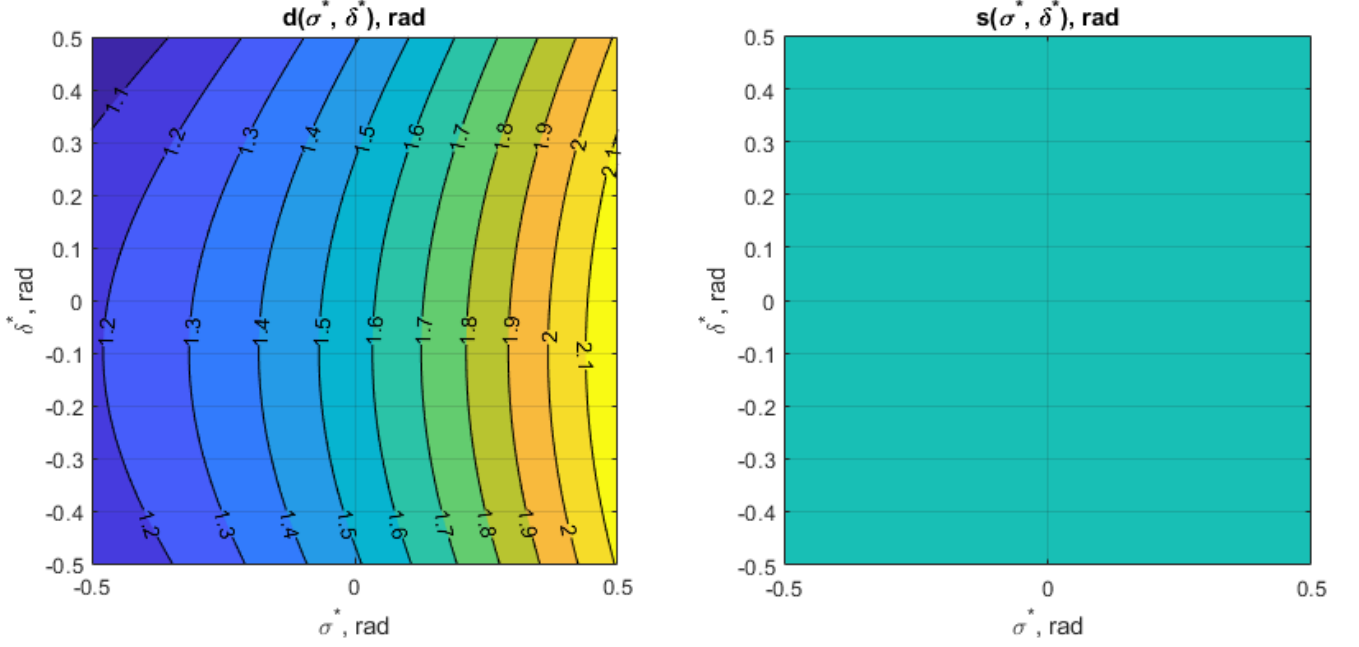


Figure 7: The switching waveform parameters  $d$  and  $s$  as functions of required  $\sigma$  and  $\delta$  for buck mode  $G = 0.5$  and  $s_{add} = 0.2$  (resulting in  $s = 0$ )

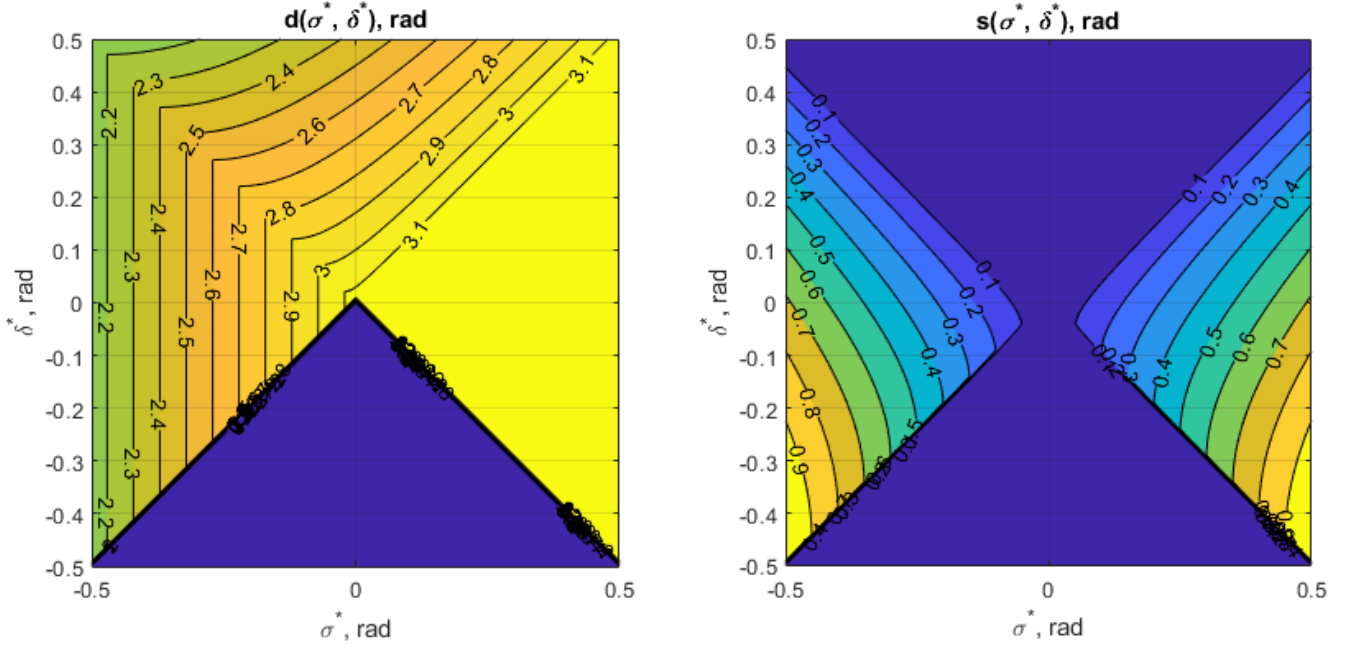


Figure 8: The switching waveform parameters  $d$  and  $s$  as functions of required  $\sigma$  and  $\delta$  for  $G = 1$  and  $s_{add} = 0$

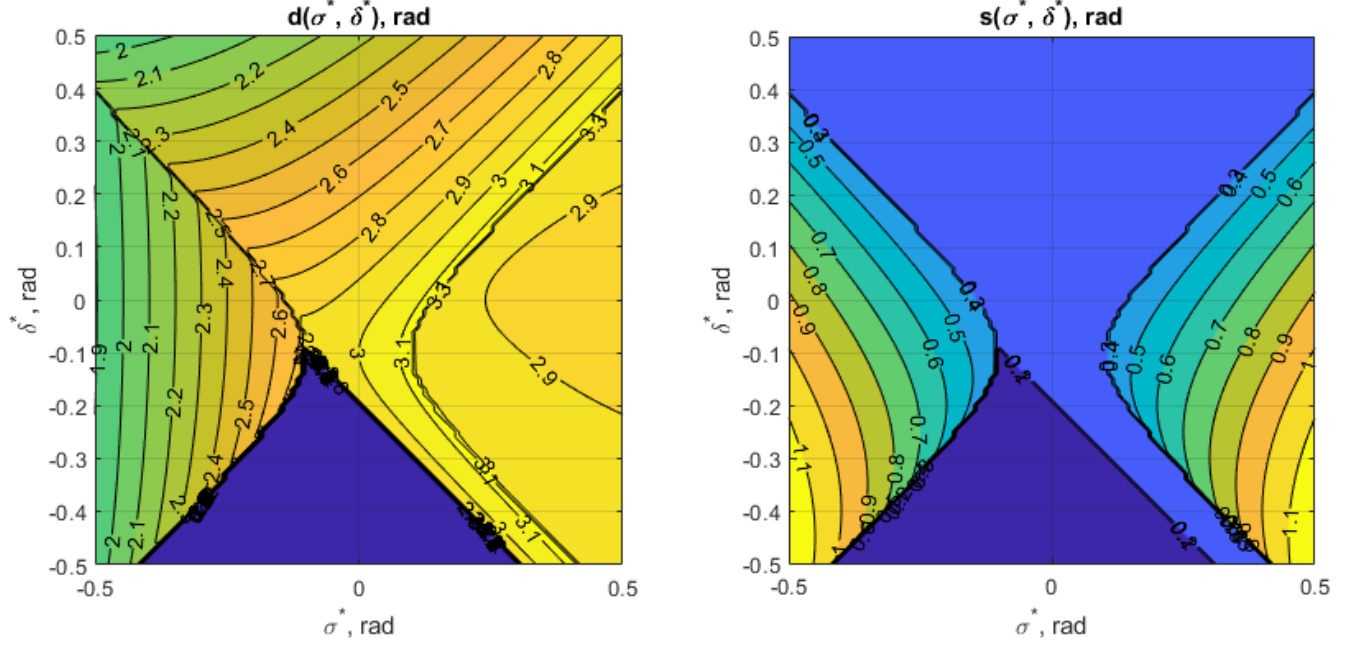


Figure 9: The switching waveform parameters  $d$  and  $s$  as functions of required  $\sigma$  and  $\delta$  for  $G = 1$  and  $s_{add} = 0.2$

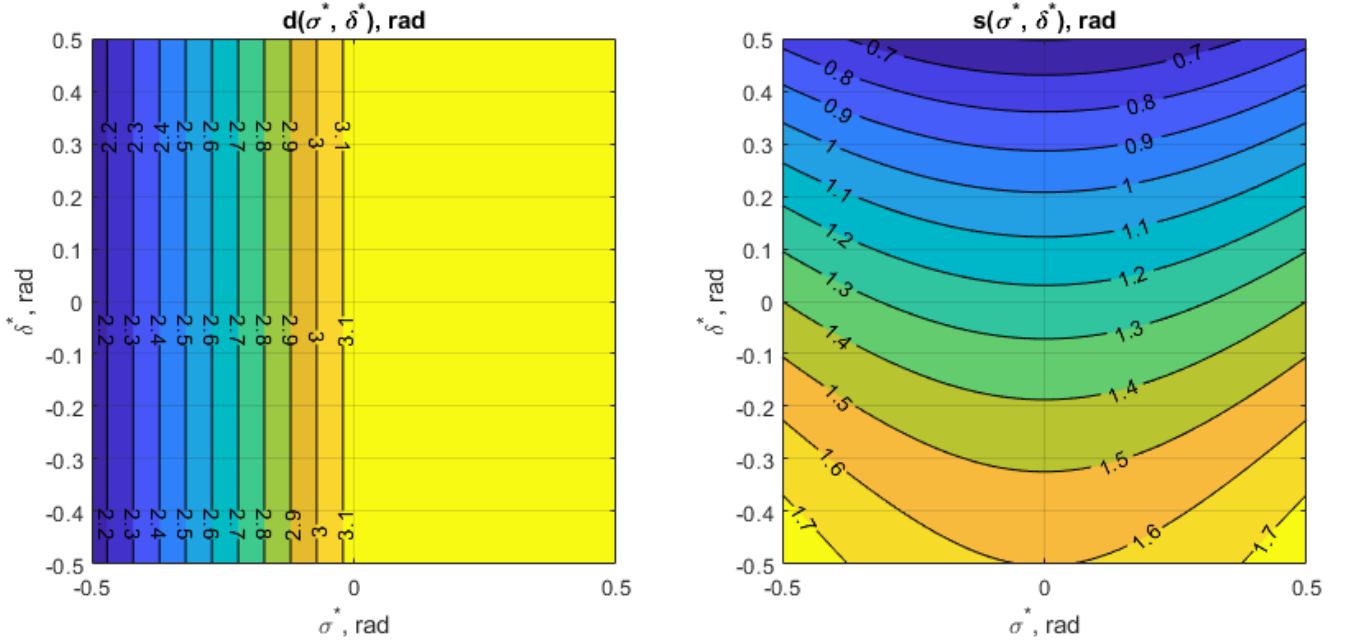


Figure 10: The switching waveform parameters  $d$  and  $s$  as functions of required  $\sigma$  and  $\delta$  for boost mode  $G = 1.5$  and  $s_{add} = 0$

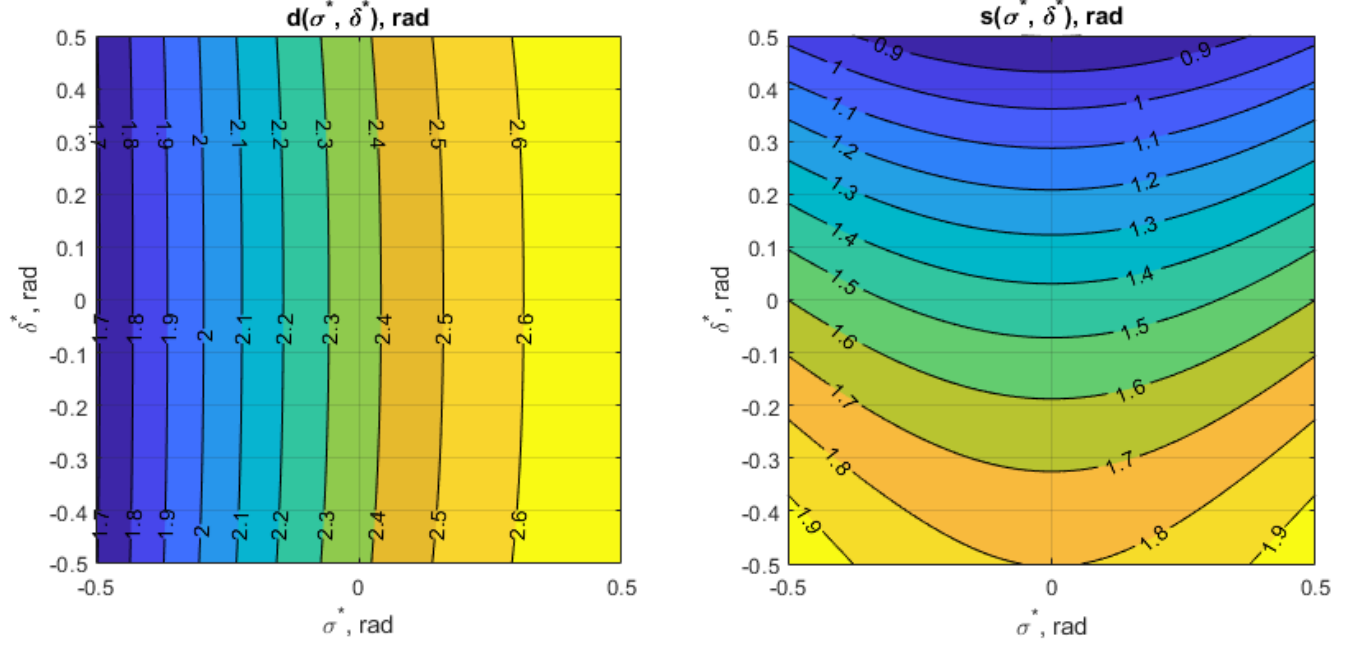


Figure 11: The switching waveform parameters  $d$  and  $s$  as functions of required  $\sigma$  and  $\delta$  for boost mode  $G = 1.5$  and  $s_{add} = 0.2$

### 3.4 Simulation of the feed-forward control

The proposed feed-forward control (41), (42) is simulating along with the plant steady-state model (3) in order to illustrate the control trajectories of PWM quantities  $d, s, \beta$ . In this simulation a sinusoidal reference trajectories are generated for  $\sigma^*, \delta^*, s_{add}$ . The  $G$  swept from 0 to 2 in time so that  $G = t$ .

The results are presented in Figures below

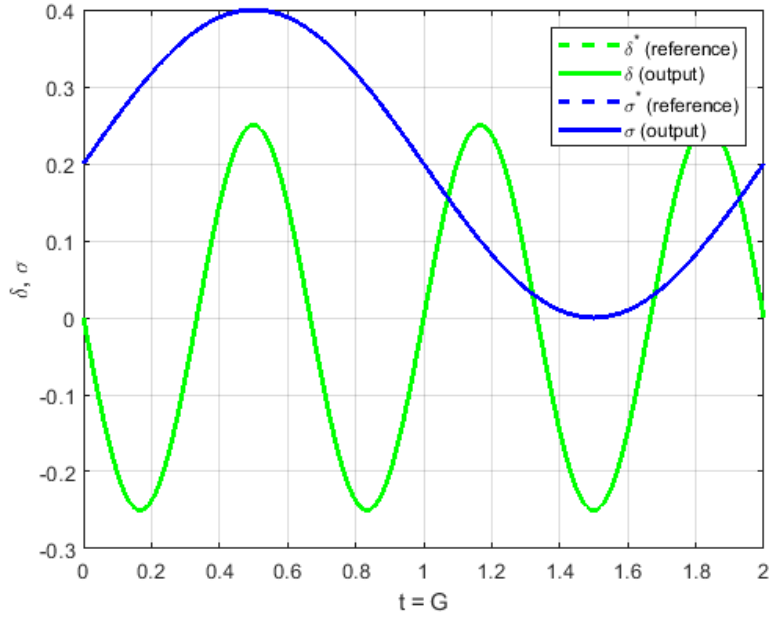


Figure 12: Simulated trajectories of  $\sigma$  and  $\delta$ : corresponding reference and output curves are overlapping

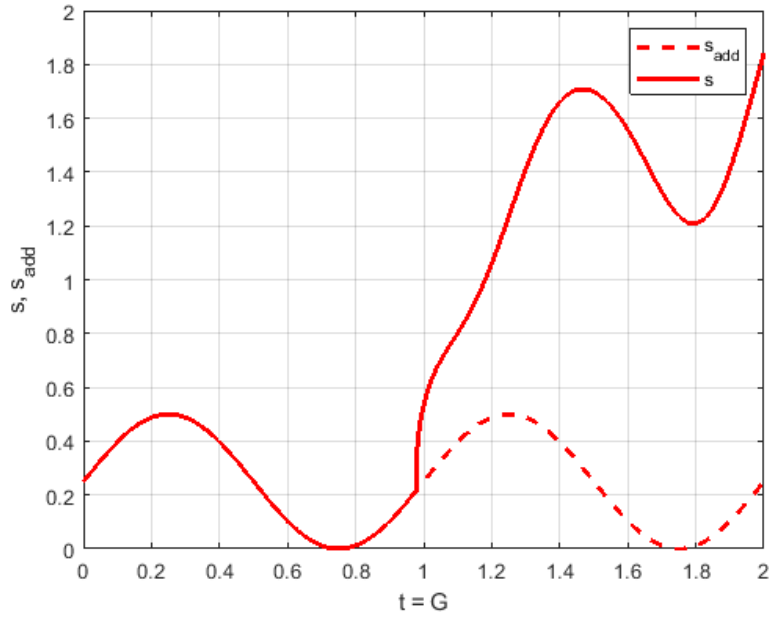


Figure 13: Simulated trajectories of  $s$  and  $s_{add}$ :  $s_{add} = s$  for buck mode  $G < 1$

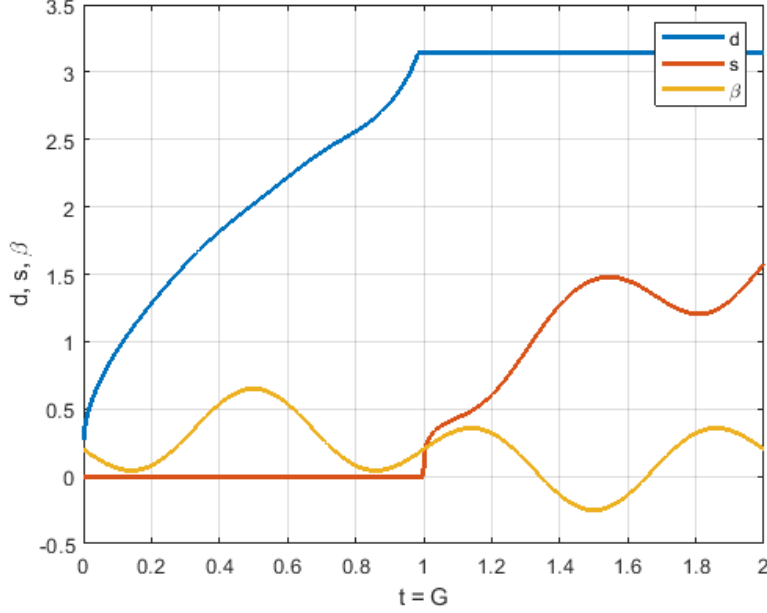


Figure 14: Simulated trajectories of control inputs  $s, d, \beta$

### 3.5 Special cases

#### 3.5.1 Special case of $G = 1$

It is important to discuss case of  $G = 1$ , because this operating point has unique properties. Furthermore, it is possible to show that  $G = 1$  is most efficient operating point with respect to the active losses in the circuit.

Substituting  $G = 1$ ,  $s_{add} = 0$  and  $\delta^* = 0$  to (42) and (41) gives:

$$\begin{aligned} s &= \arccos(2 \cos \sigma^* - 1) \\ d &= \arccos(\cos \sigma^* - 2) + \sigma^* \end{aligned} \quad (43)$$

It is pretty obvious that  $s = 0$  and  $d = \pi$  for  $\sigma^* = 0$ , along with  $\beta = 0$ . Then calculating coefficients  $A$  and  $B$  by (3) gives:  $A = 0$  and  $B = 0$ . Thus, the amplitude of tank current is  $I_t = 0$  according to (13). This leads to an important conclusion: in order to prevent collapse of tank current amplitude, the reference value of  $\sigma^*$  should be non-zero:  $\sigma^* > 0$ .

#### 3.5.2 Ideal synchronous rectification with $\delta = 0$

Let's consider second equation in (2). In order to satisfy the control goal  $\delta = 0$  for synchronous rectification, the following should be true:

$$\delta = \beta - \sigma = 0 \quad (44)$$

which gives trivially

$$\beta = \sigma \quad (45)$$

or

$$\tan \beta = \tan \sigma \quad (46)$$

or expanding by using (3) and considering only  $\tan \beta$  in the left hand side:



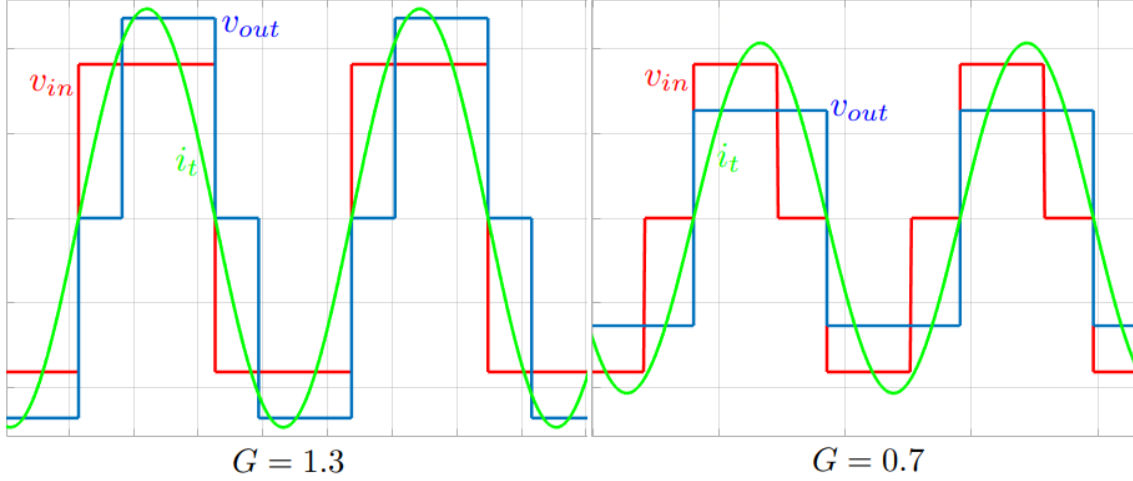


Figure 15: Voltage and current waveforms aligned with  $\beta = 0$  for buck ( $G = 0.7$ ) and boost ( $G = 1.3$ ) voltage ratios (under the same input voltage and frequency)

$$\frac{\sin \beta}{\cos \beta} = \frac{B}{A} = \frac{1 - G \cos(\beta + s) - G \cos \beta - \cos d}{\sin d + G \sin(\beta + s) + G \sin \beta} \quad (47)$$

After some trivial simplification, the last equation can be simplified down to the following, which we will call *synchronous rectification condition*:

$$\cos \beta - G - \cos(\beta - d) - G \cos s = 0 \quad (48)$$

### 3.5.3 Edge case of $\beta = 0$

As discussed earlier, it is beneficial to bring primary and secondary voltage waveforms close to each other in order to minimize commutation current. Such approach is not always practical since the current might be not enough to ensure ZVS commutation. However, this case is interesting in terms of theoretical analysis of converter characteristics.

Substituting  $\beta = 0$  into (48) immediately gives:

$$1 - G - \cos d - G \cos s = 0 \quad (49)$$

Since from the previous section,  $\sigma = \beta$  then the equation (49) describes a case when both input and output waveforms are brought together.

It is interesting to study domain of arguments for (49). The equation can be resolved with respect to  $d$ :

$$d = \arccos(1 - G - G \cos s) \quad (50)$$

and in the same time can be resolved with respect to  $s$ :

$$s = \arccos\left(\frac{1 - \cos d}{G} - 1\right) \quad (51)$$

Lets consider two cases:

- $s = 0$

From (50), the following is evident:

$$d = \arccos(1 - 2G) \quad (52)$$

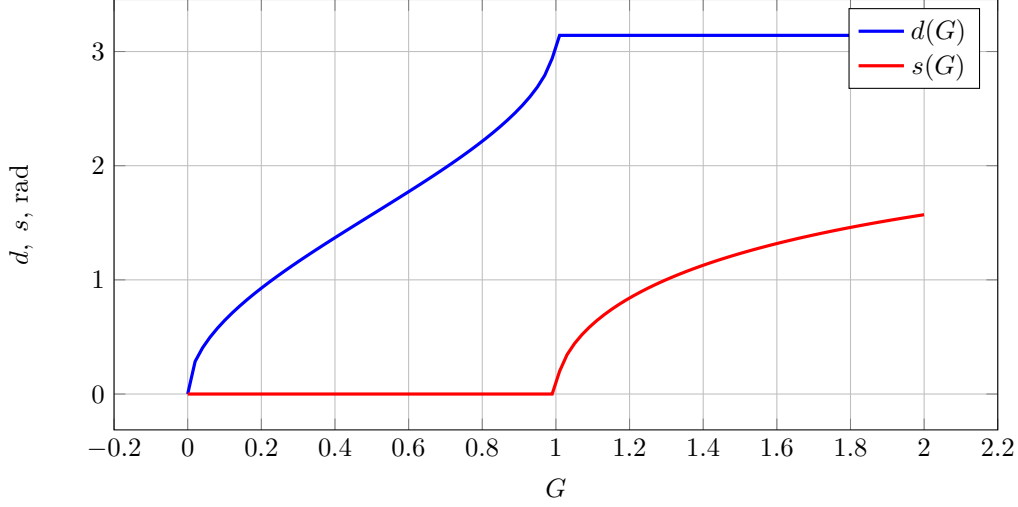


Figure 16: Maps of  $d(G)$  and  $s(G)$

which is defined on interval  $0 \leq G \leq 1$ .

If  $G = 1$ , then  $d = \pi$ .

It is also easy to see that when  $d = \pi$  or  $1 - G - G \cos s = -1$ , then  $\cos s = 2/G - 1$  and  $s$  increases with the increase of  $G \geq 1$ .

- $d = \pi$

From (51), the following is evident:

$$s = \arccos\left(\frac{2}{G} - 1\right) \quad (53)$$

which is defined on interval  $G \geq 1$ .

The combined characteristics of  $d(G)$  and  $s(G)$  are shown in Figure 16

It is possible to combine both feedforward control laws (52) and (53) into the single one by introducing a new artificial variable  $q$  piecewise parametrized by  $G$  and defined as follows:

$$q(d, s) = \begin{cases} d, & d < \pi \\ s + \pi, & d = \pi \end{cases} = \begin{cases} d, & G \leq 1 \\ s + \pi, & G > 1 \end{cases} \quad (54)$$

with the following inverse mapping back to  $d$  and  $s$ :

$$d(q) = \begin{cases} q, & G \leq 1 \\ \pi, & G > 1 \end{cases}, \quad s(q) = \begin{cases} 0, & G \leq 1 \\ q - \pi, & G > 1 \end{cases} \quad (55)$$

In the following two subsections we are going to study how the commutation angle parameters dependent from  $q$  (or  $d, s$ ), if the feedforward inversion by (52) and (53) is not exact.

### 3.5.4 Primary side fully driven converter

In two subsections below a special case of the PWM modulation with fully driven primary side will be discussed. The operating mode of primary input bridge is the same as for the conventional LLC converter. However, with a control of secondary side duty cycle  $s$  it is possible to obtain a boost operating mode and significantly increase voltage range of the converter.

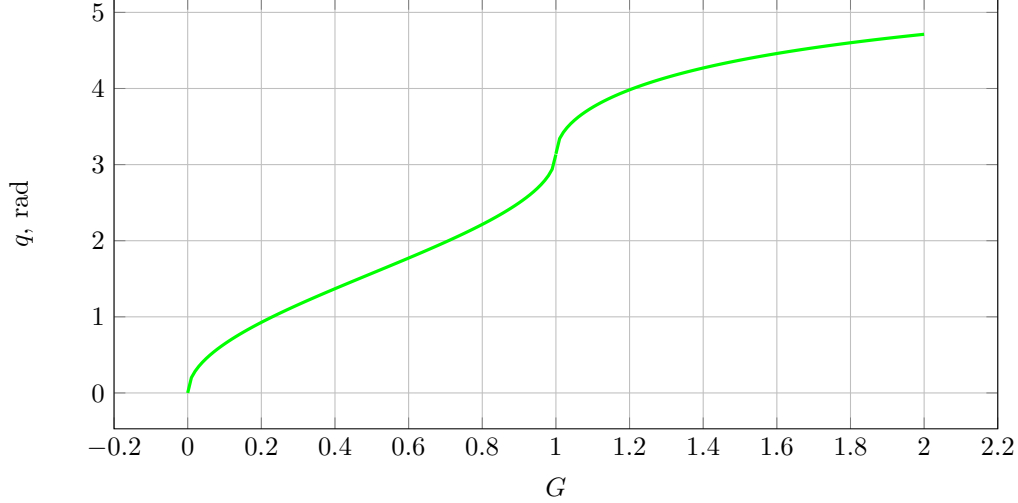


Figure 17: Map of  $q(G)$

Technically, driving the converter in this PWM type of modulation will give a slightly worse efficiency (because the primary bridge is being switched at higher instantaneous current), but this type of modulation might be desirable for EMI purposes, because the switching voltage has fewer harmonics.

Everywhere in this section we will assume  $d = \pi$ .

**Buck mode with  $d = \pi$  and  $s = 0$ .** Let's consider first a buck mode with  $s = 0$ , which corresponds to a fully driven converter on primary side and a synchronous rectification on the secondary side. Obviously, buck mode is optimal in terms of  $s \rightarrow \min$ , since 0 is minimal possible value of  $s$ .

From (48) follows that since  $\cos s = 1$ , then

$$\beta = \sigma = \arccos G \quad (56)$$

It immediately follows that in order to have a real solution for  $\beta$ , the voltage ratio should be  $G \leq 1$ , which coincides with the buck mode of converter operation.

To satisfy control goal constraint  $\sigma \geq \sigma_{min}$ , additional consideration should be imposed for voltage ratio  $G$ :

$$\begin{aligned} \sigma &\geq \sigma_{min} \\ \arccos G &\geq \sigma_{min} \\ G &\leq \cos(\sigma_{min}) \end{aligned} \quad (57)$$

Thus, as long as  $G \leq \cos(\sigma_{min})$ , the buck mode control with  $s = 0$  can satisfy goal constraint  $\sigma \geq \sigma_{min}$ , and voltage ratio  $G = \cos(\sigma_{min})$  is a boundary between buck and boost modes of converter operation.

**Boost mode with  $d = \pi$  and  $s > 0$ , buck-boost transition.** The boost mode is activated when the buck mode with  $s = 0$  is no longer capable to satisfy the control goal for  $\sigma$ , and as it was established in previous section, for  $G \geq \cos(\sigma_{min})$  a boost mode should be used. In order to satisfy optimality condition  $s \rightarrow \min$ , the  $\sigma$  should be fixed in boost mode, and we have following control problem for angles:

$$\begin{aligned} \delta &= 0 \\ \sigma &= \sigma_{min} \end{aligned} \quad (58)$$

or

$$\sigma = \beta = \sigma_{min} \quad (59)$$

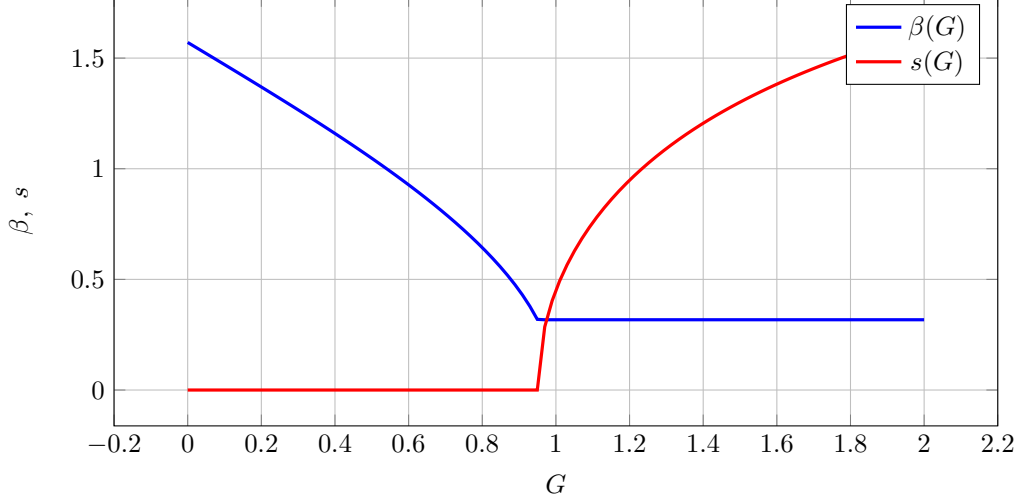


Figure 18: Maps of  $\beta(G)$  and  $s(G)$  for particular  $G^* = 0.95$

From (48) the shorting time  $s$  is determined by:

$$s = \text{acos}(2 \cos(\sigma_{min})/G - 1) \quad (60)$$

Note for the particular voltage ratio  $G = \cos(\sigma_{min})$ , i.e. exactly at the buck to boost transition border, the  $s = 0$  according to (60), which proofs continuity of  $s(G)$  function. The same is for  $\beta$ , since  $\beta = \text{acos } G$  in buck mode, then at critical voltage ratio  $G = \cos(\sigma_{min})$  we are obtaining  $\beta = \text{acos } \cos(\sigma_{min}) = \sigma_{min}$ , which coincides with continuity of  $\beta(G)$  function.

We can combine  $\beta$  and  $s$  maps for both buck and boost modes by stitching (56), (59) and (60) using minimum and maximum functions (result is pictured in Figure 18):

$$\begin{aligned} \beta &= \text{acos}(\min\{G, G^*\}) \\ s &= \text{acos}\left(\frac{2G^*}{\max\{G, G^*\}} - 1\right) \end{aligned} \quad (61)$$

where

$$G^* = \cos(\sigma_{min}) \quad (62)$$

### 3.5.5 Linearization around $\delta^* = 0$ and $\sigma^* = 0$

Even though the approach presented in this paper doesnt rely on any kind of linearization (except harmonic truncation for the first harmonic linearization), it is interesting to examine behaviour of the linearization maps around steady-state point of  $\delta^* = 0$  and  $\sigma^* = 0$ .

Lets assume  $s_{add} = 0$  for simplicity and lets linearize (25) and (32) around  $\delta^* = 0$  and  $\sigma^* = 0$ :

$$\begin{aligned} d &= d(\delta^*, \sigma^*) \approx d(0, 0) + \left. \frac{\partial d}{\partial \delta} \right|_{\delta=0} \cdot \delta^* + \left. \frac{\partial d}{\partial \sigma} \right|_{\sigma=0} \cdot \sigma^* = \\ &= \text{acos}(1 - 2G) - \left. \frac{G \sin \delta}{\sqrt{G(1-G)}} \right|_{\delta=0} \cdot \delta^* + \left. \frac{\sin \sigma}{2\sqrt{G(1-G)}} \right|_{\sigma=0} \cdot \sigma^* + \sigma^* \end{aligned} \quad (63)$$

$$\begin{aligned} s &= s(\delta^*, \sigma^*) \approx s(0, 0) + \delta^* \left. \frac{\partial s}{\partial \delta} \right|_{\delta=0} + \sigma^* \left. \frac{\partial s}{\partial \sigma} \right|_{\sigma=0} = \\ &= \pi - \text{acos}(1 - 2/G) - \left. \frac{G \sin \delta}{2\sqrt{G-1}} \right|_{\delta=0} \cdot \delta^* + \left. \frac{\sin \sigma}{\sqrt{G-1}} \right|_{\sigma=0} \cdot \sigma^* - \delta^* \end{aligned} \quad (64)$$

Thus, in trivial case, the decoupling transformation can be approximated as follows:

$$\begin{aligned} d &= \begin{cases} \arccos(1 - 2G) + \sigma^*, & G < 1 \\ \pi, & G > 1 \end{cases} \\ s &= \begin{cases} 0, & G < 1 \\ \pi - \arccos(1 - 2/G) - \delta^*, & G > 1 \end{cases} \\ \beta &= \sigma^* + \delta^* \end{aligned} \quad (65)$$

This transformation is not defined at  $G = 1$ , because according to section 3.5.1,  $\sigma^* > 0$  in order to prevent tank current from collapse to zero. Also according to (63) and (64), partial derivatives  $\partial d/\partial \delta$ ,  $\partial d/\partial \sigma$ ,  $\partial s/\partial \delta$ ,  $\partial s/\partial \sigma$  are all singular near  $G = 1$ .

It worth noting that this (65) is only an approximation of exact inversion (25) and (32). An external feedback controller has to be used in order to achieve satisfactory results. This can be illustrated by the same time of simulation performed in section 3.4, presented in Figures below [].

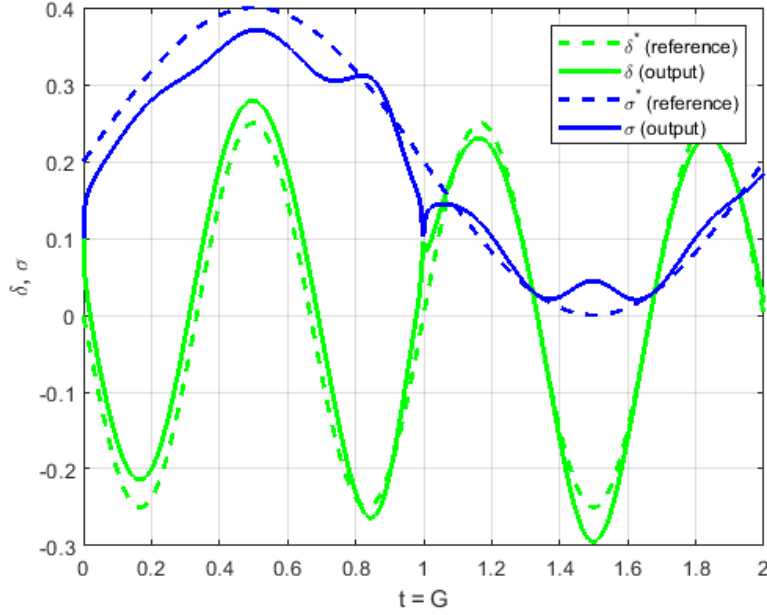


Figure 19: Simulated trajectories of  $\sigma$  and  $\delta$  without external feedback controller, only using linear map (65)

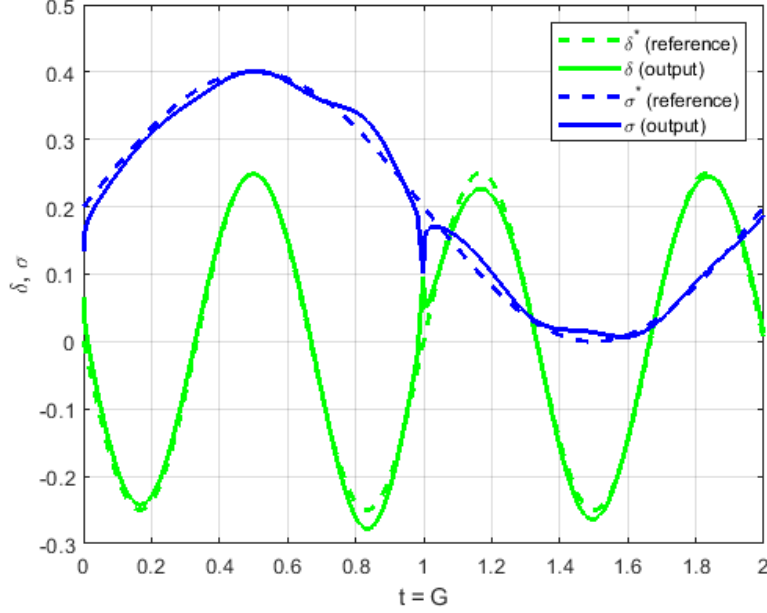


Figure 20: Simulated trajectories of  $\sigma$  and  $\delta$  using individual PI controllers in addition to feed-forward term (65)

The conclusions from the simulation results are: introduction of PI controllers are enhancing regulation accuracy in comparison to purely feed-forward control (65), also the control trajectories have cusp in  $G = 1$ , which was expected.

## 4 Output power control

### 4.1 Variable frequency control

According to (2) the output current control can be formulated in terms of transconductance  $W$  by simply multiplying it by input voltage  $V_{in}$ :  $I_{out} = WV_{in}$ . Thus, the output current can be regulated by means of transconductance regulation by satisfying the following control goal:

$$W = W^* \quad (66)$$

where  $W^* = I_{out}^*/V_{in}$ , and  $I_{out}^*$  is referenced output current.

Let's assume that commutation parameters  $d, s, \beta$  are at their steady-states, defined by controls (25) and (32) or corresponding special cases, discussed in the previous chapter. That means that coefficients  $A$  and  $B$  from (3) can be parametrized in terms of reference values  $\sigma^*$  and  $\delta^*$ , along with  $s_{add}$  (if this feature is used):

$$\begin{aligned} A &= 4 \sin d(\sigma^*, \delta^*, s_{add}) + 4G \sin(\sigma^* + \delta^* + s(\sigma^*, \delta^*, s_{add})) + 4G \sin(\sigma^* + \delta^*) = A(\sigma^*, \delta^*, s_{add}, G) \\ B &= 4 - 4G \cos(\sigma^* + \delta^* + s(\sigma^*, \delta^*, s_{add})) - 4G \cos(\sigma^* + \delta^*) - 4 \cos d(\sigma^*, \delta^*, s_{add}) = B(\sigma^*, \delta^*, s_{add}, G) \end{aligned} \quad (67)$$

Based on this, the transconductance (2) can be separated into two parts  $H$  and  $Z$ : one is parametrized by reference commutation parameters  $\sigma^*, \delta^*, s_{add}$  and another one by switching frequency  $\omega$ .

$$W = \frac{I_{out}}{V_{in}} = \frac{n}{2\pi^2} \frac{H(\sigma^*, \delta^*, s_{add}, G)}{Z(\omega)} \quad (68)$$

where

$$H = \sqrt{A^2 + B^2} \cdot (\cos(s + \delta) + \cos \delta) \quad (69)$$

Then the frequency control consists of calculation of  $\omega$  which satisfies (68) for a given referenced  $W^*$ . The (68) can be solved with respect to  $Z(\omega)$ :

$$Z = \frac{n}{2\pi^2} \frac{H(\sigma^*, \delta^*, s_{add}, G)}{W^*} \quad (70)$$

And in the same time  $Z(\omega) = \omega L - 1/(\omega C)$ , from here the required  $\omega$  can be easilly obtained:

$$\omega = \frac{1}{2LC} \left( \sqrt{C^2 Z^2 + 4LC} + CZ \right) \quad (71)$$

## 4.2 Special case for fully driven converter

The output transconductance with feed-forward maps  $\cos \beta = G$  and  $\delta = 0$  can be calculated as after all simplifications using (56) and  $s = 0$ :

$$W = \frac{8n}{\pi^2} \frac{1}{Z(\omega)} \sqrt{1 - G^2} \quad (72)$$

Let's calculate frequency  $\omega$  which is needed to achieve desired output  $W_{ref}$ :

$$Z = \frac{8n\sqrt{1 - G^2}}{\pi^2 W_{ref}} \omega = \frac{1}{2LC} \left( \sqrt{C^2 Z^2 + 4LC} + CZ \right) \quad (73)$$

The combined feed-forward control law (both for buck and boost modes) can be formulated as follows: For given  $W_{ref}$  and  $G$ , and also pre-calculated buck to boost threshold  $G^* = \cos(\sigma_{min})$ :

1. First calculate the control inputs  $\beta$  and  $s$

$$\begin{aligned} \beta &= \arccos(\min\{G, G^*\}) \\ s &= \arccos\left(\frac{2G^*}{\max\{G, G^*\}} - 1\right) \end{aligned} \quad (74)$$

2. Then calculate desired tank impedance:

$$Z = 4n \frac{\cos s + 1}{\pi^2 W_{ref}} \sqrt{1 - G \cos(\beta + s)} \quad (75)$$

3. The switching frequency will be determined by equation:

$$\omega = \frac{1}{2LC} \left( \sqrt{C^2 Z^2 + 4LC} + CZ \right) \quad (76)$$

## 4.3 Low power mode with $\omega = \omega_{max}$

The switching frequency in control (73) is unbounded, i.e. in order to get  $W^* = 0$  frequency should be  $\omega \rightarrow \infty$ . In real systems, the upper frequency is always constrained at  $\omega_{max}$ . Thus if we need output power even lesser than we can get at  $\omega = \omega_{max}$ , impedance can't be further increased and control of output power can be achieved only by commutation parameters  $s$  and  $\beta$  with fixed  $\omega = \omega_{max}$ . This mode we will call a low power mode.

Let's define maximum impedance that we can get:

$$Z_{max} = \omega_{max} L - \frac{1}{\omega_{max} C} \quad (77)$$

The control law for low power can be formulated as follows: for a given  $W^*$  find commutation parameters  $d, s, \beta$  which are satisfying following conditions:

$$W^* = \frac{n}{2\pi^2} \frac{H(\sigma^*, \delta^*, s_{add}, G)}{Z(\omega)} \quad (78)$$

Let's consider an idea to limit output power by additional increase of  $s$ , which is equivalent to dimming the output down to zero power at  $s = \pi$  when secondary side is completely shorted. Just to mention that another possibility for output power regulation at constant frequency is to shift the secondary side respect to primary side by introducing  $\delta > 0$ .

For implementation of this idea the  $s_{add}$  was introduced in section 3.2.3 which resulted in inversion maps (25) and (32).

As stated by equation (48), for any arbitrary  $s$  in synchronous rectification:

$$\cos \beta = \frac{G}{2}(\cos s + 1) \quad (79)$$

By using equation (48) and denoting  $x = \cos s$  the equation (78) can be simplified down to:

$$W_{ref} = 2\sqrt{2}n \frac{x+1}{\pi^2 Z_{max}} \sqrt{G\sqrt{(1-x^2)(4-G^2(x+1)^2)} - G^2x(x+1) + 2} \quad (80)$$

which is algebraic respect to  $x$ .

To characterize dependency of  $W$  from  $s$  with fixed frequency, let's try to calculate (80) for different values of  $G$ . Let's denote  $s_0$  and  $\beta_0$  as commutation parameters obtained by (74) without any additional secondary side shorting for low power. Likewise, let's denote  $W_0$  the output power obtained for fixed maximal frequency  $\omega_{max}$ , but without any additional secondary side shorting for low power.

$$W_0 = 4n \frac{\cos s_0 + 1}{\pi^2 Z_{max}} \sqrt{1 - G \cos(\beta_0 + s_0)} \quad (81)$$

The output power variation for different values of  $G$  is demonstrated in Figure 21 as ratio of  $W/W_0$ . As one can see from the picture, the zero power operation  $W = 0$  is achieved for  $s = \pi$  (fully shorted secondary side) regardless of  $G$ . But an interesting feature of the system is that  $W = W_0$  can be seen for the values  $s > 0$  even in buck mode. That means that the characteristic  $W(s)$  is non-monotonic, and a discontinuous control will be applied for  $s$  when transitioning from regular operation (with  $W_0$  output power) to a low power operation with  $W < W_0$ . This feature will be addressed separately later.

The final algorithm for feed-forward map calculations in low power mode is formulated as follows:

*If calculated switching frequency in control (73) greater than  $\omega_{max}$  to obtain a desired  $W_{ref}$ , then*

*1. Numerically solve following equation for  $x$ :*

$$2\sqrt{2}n \frac{x+1}{\pi^2 Z_{max}} \sqrt{G\sqrt{(1-x^2)(4-G^2(x+1)^2)} - G^2x(x+1) + 2} = W_{ref} \quad (82)$$

*The solution can be obtained using bisection (dichotomy) method by ranging  $x \in [-1, \cos s_0]$ .*

*2. Calculate switching parameters as follows:*

$$\begin{aligned} s &= \arccos x \\ \beta &= \arccos \left( G \cdot \frac{x+1}{2} \right) \end{aligned} \quad (83)$$

## References

- [1] Li, X. and Bhat, A.K., 2010. Analysis and design of high-frequency isolated dual-bridge series resonant DC/DC converter. IEEE Transactions on Power Electronics, 25(4), pp.850-862.
- [2] Krismer, F., Biela, J. and Kolar, J.W., 2005, October. A comparative evaluation of isolated bi-directional DC/DC converters with wide input and output voltage range. In Industry Applications Conference, 2005. Fourtieth IAS Annual Meeting. Conference Record of the 2005 (Vol. 1, pp. 599-606). IEEE.
- [3] Wang, C.S., Li, W., Wang, Y.F., Han, F.Q., Meng, Z. and Li, G.D., 2017. An Isolated Three-Port Bidirectional DC-DC Converter with Enlarged ZVS Region for HESS Applications in DC Microgrids. Energies, 10(4), p.446.



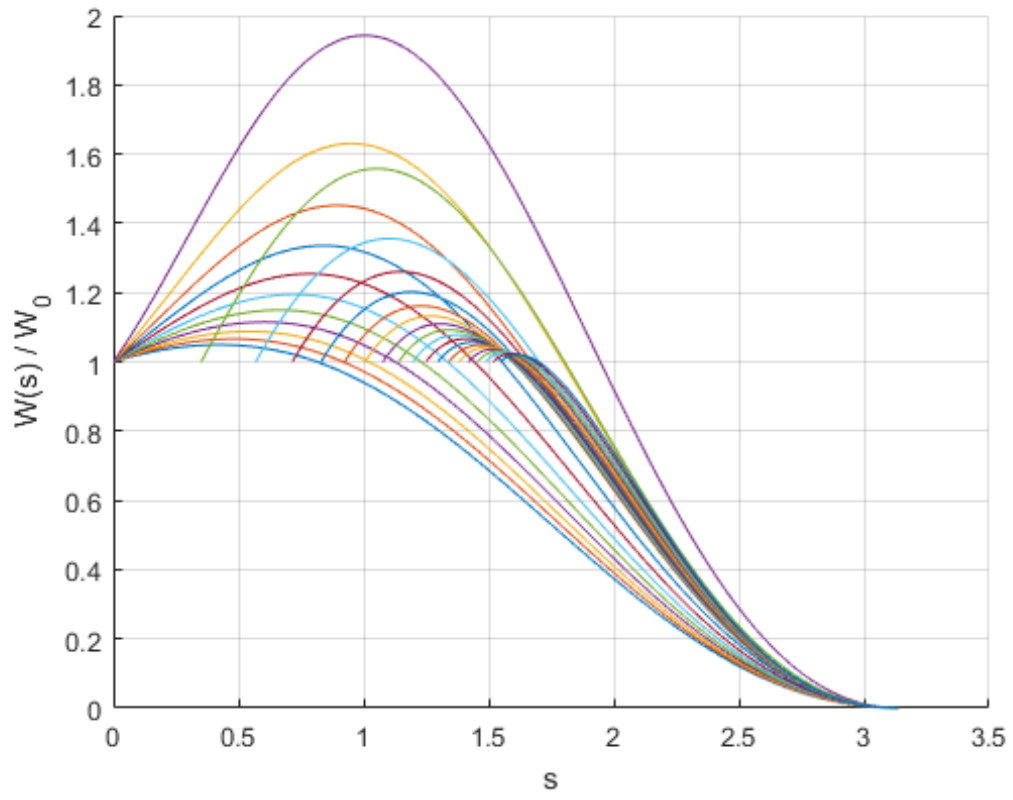


Figure 21: Output power variation with  $s$  ranging from  $s_0$  to  $\pi$  for  $0.4 \geq G \geq 1.8$

- [4] Zhao, B., Song, Q., Liu, W. and Sun, Y., 2014. Overview of dual-active-bridge isolated bidirectional DC-DC converter for high-frequency-link power-conversion system. *IEEE Transactions on Power Electronics*, 29(8), pp.4091-4106.
- [5] <https://www.fairchildsemi.com/application-notes/AN/AN-4151.pdf>
- [6] Hu, S., Li, X., Lu, M. and Luan, B.Y., 2015. Operation Modes of a Secondary-Side Phase-Shifted Resonant Converter. *Energies*, 8(11), pp.12314-12330.
- [7] Jiang, M. and Li, W., 2014. A Soft-Switching Control Method of Isolated LC Series Resonant Transformer Full Bridge DC-DC Converter. In *Proceedings of the 2013 International Conference on Electrical and Information Technologies for Rail Transportation (EITRT2013)-Volume II* (pp. 11-20). Springer, Berlin, Heidelberg.
- [8] Wu, H., Wang, P. and Li, Y., 2014, August. A control method for series resonant dual active bridge DC/DC converter. In *Transportation Electrification Asia-Pacific (ITEC Asia-Pacific), 2014 IEEE Conference and Expo* (pp. 1-5). IEEE.
- [9] Hu, G.-Y.; Li, X.; Luan, B.-Y., 2014. A Generalized Approach for the Steady-State Analysis of Dual-Bridge Resonant Converters. *Energies* 2014, 7, 7915-7935.
- [10] Chen, H. and Bhat, A.K., 2016, May. A bidirectional dual-bridge LCL-type series resonant converter controlled with modified gating scheme. In *Power Electronics and Motion Control Conference (IPEMC-ECCE Asia), 2016 IEEE 8th International* (pp. 3036-3042). IEEE.
- [11] Aboushady, A.A., Ahmed, K., Finney, S.J. and Williams, B.W., 2010. Steady-state analysis of full-bridge series resonant converter with phase-shift and frequency control. In *Power Electronics, Machines and Drives (PEMD 2010), 5th IET International Conference on*, 2010, pp 1-6.
- [12] Oruganti, R., 1987. State-plane analysis of resonant converters (Doctoral dissertation, Virginia Polytechnic Institute and State University).
- [13] Rossetto, L., 1996. A simple control technique for series resonant converters. *IEEE Transactions on Power Electronics*, 11(4), pp.554-560.
- [14] Chen, H., Sng, E.K.K. and Tseng, K.J., 2006. Generalized optimal trajectory control for closed loop control of series-parallel resonant converter. *IEEE transactions on power electronics*, 21(5), pp.1347-1355.
- [15] Feng, W., Lee, F.C. and Mattavelli, P., 2013. Simplified optimal trajectory control (SOTC) for LLC resonant converters. *IEEE Transactions on Power Electronics*, 28(5), pp.2415-2426.
- [16] Sarnago, H., Lucia, O., Mediano, A. and Burdio, J.M., 2015. Analytical model of the half-bridge series resonant inverter for improved power conversion efficiency and performance. *IEEE Transactions on Power Electronics*, 30(8), pp.4128-4143.
- [17] Jiang, J., Bao, Y. and Wang, L.Y., 2014. Topology of a bidirectional converter for energy interaction between electric vehicles and the grid. *Energies*, 7(8), pp.4858-4894.
- [18] Zhao, X., Zhang, L., Born, R. and Lai, J.S., 2017. A high-efficiency hybrid resonant converter with wide-input regulation for photovoltaic applications. *IEEE Transactions on Industrial Electronics*, 64(5), pp.3684-3695.
- [19] Riedel, J. 2017. On frequency domain analysis of dual active bridge dc-dc converters. Ph.D. thesis, RMIT Melbourne, Dissertation, March 2017.
- [20] Xiao, Y., Zhang, Z., Mao, X., Manez, K.T. and Andersen, M.A., 2018, March. Power plateau and anti-power phenomenon of dual active bridge converter with phase-shift modulation. In *Applied Power Electronics Conference and Exposition (APEC), 2018 IEEE* (pp. 1871-1875). IEEE.

- [21] Shen, Y., Wang, H., Al-Durra, A., Qin, Z. and Blaabjerg, F., 2018. A Bidirectional Resonant DC–DC Converter Suitable for Wide Voltage Gain Range. *IEEE Transactions on Power Electronics*, 33(4), pp.2957-2975.
- [22] Borisevich, A., and Gleyzer, F., 2019. Model of DC/DC Dual-Bridge Series Resonant Converter in Buck and Boost Modes for Output Current and Commutation Timing Control. *Journal of Engineering Science and Technology Review* 12.2 (2019): 152-160.
- [23] J. C. Hertel, J. E. F. Overgaard, I. H. H. Jørgensen, T. M. Andersen, M. Rødgaard and A. Knott, "Synchronous Rectifier for High-Frequency Switch-Mode Power Supplies Using Phase-Locked Loops," in *IEEE Journal of Emerging and Selected Topics in Power Electronics*, vol. 8, no. 3, pp. 2227-2237, Sept. 2020, doi: 10.1109/JESTPE.2019.2945542.